Gradiometric micro-SQUID susceptometer for scanning measurements of mesoscopic samples

Martin E. Huber,[1,a)] Nicholas C. Koshnick,[2] Hendrik Bluhm,[2,b)] Leonard J. Archuleta,[1] Tommy Azua,[1] Per G. Björnsson,[2] Brian W. Gardner,[2] Sean T. Halloran,[1] Erik A. Lucero,[1,c)] and Kathryn A. Moler[2]
[1]*Department of Physics, University of Colorado Denver, Denver, Colorado 80217-3364, USA*
[2]*Geballe Laboratory for Advanced Materials, Stanford University, Stanford, California 94305-4045, USA*

(Received 19 February 2008; accepted 29 April 2008; published online 28 May 2008)

We have fabricated and characterized micro-SQUID susceptometers for use in low-temperature scanning probe microscopy systems. The design features the following: a 4.6 μm diameter pickup loop; an integrated field coil to apply a local field to the sample; an additional counterwound pickup-loop/field-coil pair to cancel the background signal from the applied field in the absence of the sample; modulation coils to allow setting the SQUID at its optimum bias point (independent of the applied field), and shielding and symmetry that minimizes coupling of magnetic fields into the leads and body of the SQUID. We use a SQUID series array preamplifier to obtain a system bandwidth of 1 MHz. The flux noise at 125 mK is approximately $0.25\mu\Phi_0/\sqrt{\text{Hz}}$ above 10 kHz, with a value of $2.5\mu\Phi_0/\sqrt{\text{Hz}}$ at 10 Hz. The nominal sensitivity to electron spins located at the center of the pickup loop is approximately $200\mu_B/\sqrt{\text{Hz}}$ above 10 kHz, in the white-noise frequency region. © *2008 American Institute of Physics.* [DOI: 10.1063/1.2932341]

I. INTRODUCTION

The magnetic response of micro- and nanometer scale objects, as a function of an applied magnetic field, reveals properties that cannot be probed directly by other methods. For instance, the current in a mesoscopic ring is the first derivative of the ring's free energy with respect to magnetic flux, allowing for the study of fundamental thermodynamic properties.[1] The periodicity of the free energy with respect to the flux quantum gives a variety of effects, including the Little–Parks effect,[2] multiple fluxoid transitions,[3] and the detection of novel superconducting wave function states.[4] The intrinsic sensitivity of superconducting quantum interference devices (SQUIDs) to magnetic flux makes these devices some of the world's best instruments for measuring magnetic fields.[5] In this paper we present a scanning SQUID susceptometer that has enabled results[1,3,4] on micrometer scale objects in part because it is specifically designed to measure the response of small objects as a function of applied field.

Micro-SQUIDs excel at quantitative measurement of small magnetic signals, including the total magnetic response to applied field (moment or susceptibility) of nanoscale objects. These measurements have traditionally been done with nonscanning sensors that are integrated onto the same chip as the sample,[6] require physical placement of a sample in the pickup loop,[7] or are used in a static flip-chip geometry.[8] Use of a scanning sensor has multiple advantages in these applications, allowing measurement of samples that are on different substrates or that can be fabricated by incompatible processes, as well as measurement of multiple samples in a single cooldown. Most importantly for the smallest signals, a scanning sensor allows *in situ* measurements of the background simply by moving away from the sample.

We report on the design, fabrication, and characterization of scanning SQUID susceptometers with 4.6 μm diameter pickup loops, integral and robust shielding, and a high degree of symmetry. Section II presents the basic design considerations. Section III briefly describes the experimental configuration, including the scanning stage and preamplifier with which we are able to achieve the same intrinsic flux sensitivity while scanning as while in a static, well-shielded environment. Section IV discusses the noise design and device performance in detail. Section V presents some representative measurements made by this device, describes the background cancellation technique, and gives the demonstrated ring-flux sensitivity.

II. DESIGN

All SQUIDs have nonlinear current-voltage characteristics with a critical current that depends periodically on the total magnetic flux Φ_{SQ} through the SQUID loop with a periodicity of the superconducting flux quantum, $\Phi_0=h/2e$. The smallest micro-SQUIDs fabricated to date are also the most basic, consisting of a simple superconducting loop with two microbridges of various types.[9–12] Because it is not possible to use a feedback circuit to keep the SQUID in a flux-locked loop if there are no modulation coils, the response of simple SQUIDs is nonlinear in applied field. In principle, a modulation coil could be added, but in practice, modulation coils have limited use because the modulation field is applied

[a)]Electronic mail: martin.huber@cudenver.edu.
[b)]Also at Department of Physics, Harvard University.
[c)]Also at Department of Physics, University of California–Santa Barbara, Santa Barbara, California.

to the sample as well. Fabricating a pickup loop that is separate from the core area of the SQUID solves both of these problems,[13] at the expense of compactness.

SQUIDs with independent control of sample flux and bias flux allow for operation at the maximum-sensitivity bias point for all measurement conditions. A pickup loop/field coil pair can be separated in space from the modulation coil to reduce cross coupling. Separating the pickup loop and the main body of the SQUID (consisting of the junctions, junction shunts, and modulation coils) also allows the pickup loop to be optimized for coupling to the sample.[14]

In many cases, it is further desirable to null the SQUID's response to the applied field so that the signal only reflects the magnetic response of the sample to the applied field. This can be done by including a separate, counterwound pickup-loop/field-coil pair to cancel the response to the applied field. Designs including such features are known as SQUID susceptometers and were first proposed and produced by Ketchen *et al.*,[7] modified to a coaxial geometry by Ketchen and Kirtley,[14] and implemented in a scanning geometry by Gardner *et al.*[15] with 8 μm diameter pickup loops.

SQUIDs are intrinsically sensitive to the magnetic flux threading their pickup area; thus, the best field sensitivity is achieved with the largest pickup area compatible with a given application. While large SQUIDs have the best sensitivity to magnetic field, small SQUIDs have better coupling to small samples. Our nominal 4 μm diameter pickup loop is chosen to balance the competing requirements of maximum sensitivity (better for smaller diameters) and of having a convenient scan/imaging kernel (which limits the minimum diameter, relative to the lithographically limited spacing between the pickup loop leads, 2 μm center to center). The measured effective diameter—that is, the geometric mean of the inner (3.95 μm) and outer (5.15 μm) diameters of the loop[16]—is 4.6 μm. This pickup loop size also results in near-optimal coupling to micrometer-scale samples, such as rings, for which fields on the order of 50 Oe can apply several Φ_0 through a given sample's center. When the sample's diameter is sufficiently small compared to the pickup loop size [Fig. 1(a)] the field lines can be approximated as an ideal dipole [Fig. 1(b)]. When the dipole moment m is in the center of the pickup loop and aligned perpendicular to the pickup loop plane as shown, the magnetic flux captured by the sensor[17] is $\Phi_{SQ}=mr_e/a$, where a is the radius of the ring, $r_e=2.8\times10^{-15}$ m is the classical electron radius, Φ_{SQ} is in units of Φ_0, and m is in units of Bohr magnetons, μ_B. Smaller pickup loops allow fewer field lines to close within the sensor area, increasing the total magnetic flux threading the loop. The coupling decreases rapidly if the dipole is more than one pickup loop radius away from the plane of the pickup loop. Maximal dipole coupling occurs when the dipole is directly next to the inner edge of the pickup loop itself, at which point the Meissner screening associated with the pickup loop linewidth can play an important role and more accurate modeling[18] is required to estimate the sensitivity to spins.

To measure the magnetic response of a sample as a function of applied field, the measurement process must cancel the sensor's response to the applied field itself. To aid this cancellation process, our susceptometer is designed with

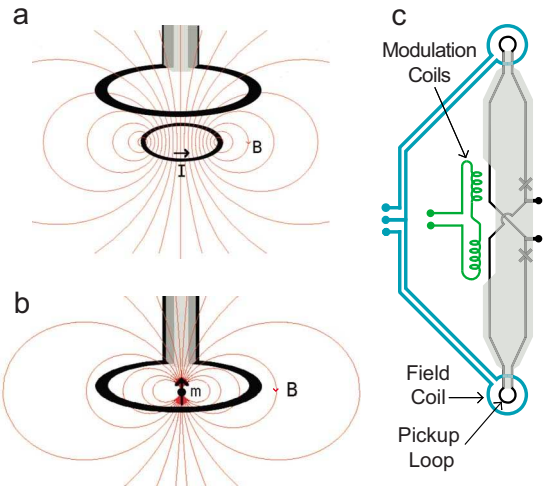

FIG. 1. (Color online) (a) Field lines from a current I in a ring positioned on axis but slightly below the pickup loop, with the shielding tab shown in gray. (b) Field lines from the dipole moment of a mesoscopic sample located at the center of a pickup loop. The flux captured by the pickup loop increases as the loop diameter decreases. The net flux also increases if the sample is moved to a position directly under the wire forming the pickup loop. (c) Simplified diagram of the device, showing the general relationship between the pickup loops, the field coils, and the modulation coils. The center tap of the field coils allows compensation of lithographic imperfections between the two pickup loops. The shading represents the low inductance planar coaxial shield on the susceptometer arms.

two, nominally identical, counterwound pickup loops. These loops are separated by 1.2 mm on the sensor chip so that one loop can be located in close proximity to the sample while the other loop is far from the sample substrate to avoid unwanted coupling [Fig. 1(c)]. The symmetry of the design leads to both a geometric cancellation of a uniform applied field and a balanced inductance between the two arms of the SQUID, which leads to improved electrical performance.

We apply field to the area near the two pickup loops with local single-turn field coils that are fully integrated into the SQUID chip layout. The effective diameter of each field coil is 13.6 μm (just slightly greater than twice the diameter of the pickup loop), resulting in a field at the center of the loop of approximately 0.1 T/A. The field coils are fabricated from a thin-film Nb layer deposited directly on the substrate so as to avoid edge crossings that might decrease the critical current of the lines. Although the critical current of the field coil, I_0^{FC}, is typically $\sim$75 mA, effective operation is limited to a smaller range $I_{max}^{FC}\lesssim\pm45$ mA due to nonlinearities that are presumed to result from the onset of vortex motion in SQUID elements.

The two field coils are connected in series, so that a constant current applies the same magnetic induction to both pickup loops. A geometric imbalance of approximately 1 part in 100 is thought to be caused by alignment imperfections in lithography. A center tap on the field coil leads allows one to cancel this residual geometric coupling between field coils and pickup loops to within 1 part in 10 000. At this level of cancellation, we are able to apply $\sim40\Phi_0$ of field with a residual signal of only a few $m\Phi_0$. This allows for sufficient dynamic range in the preamplifier/readout electronics to measure the residual background with the necessary sensitivity for postprocessing background subtraction (described later).

The local field coils have three additional advantages when compared to a system that operates in a uniform field applied by an external solenoid. First, the integrated field coils have a comparatively low inductance which enables the possibility of oscillating the applied field at a high rate (~10 kHz), alleviating many of the problems associated with low frequency sensor noise. Second, because the field from the field coils itself falls off as $1/r^3$ when the distance from the sample, r, is larger than the field coil diameter, the field from the sample at the pickup loop falls off even more rapidly, as $1/r^6$ (as opposed to $1/r^3$ for a uniform field). This situation allows for a more independent characterization of the SQUID's response to the applied field *in situ* away from any sample. Finally, the local field coils allow for the modulation coils and Josephson junctions to operate in a low field environment.

Integrated modulation coils allow for operation in a flux locked loop. The feedback technique linearizes the response in the applied flux and allows the SQUID to operate at a flux bias point of optimal sensitivity[5] in all applied fields at the sample. The modulation coils are larger than the applied field coils, reducing the feedback current requirements, and thus the heating from stray resistances in the low temperature wiring. Although the region of the SQUID that couples to the modulation coils will cancel constant background fields with its gradiometric design, it is still sensitive to gradients in the applied field due to its large size. We find that scanning mount vibrations of approximately 25 nm magnitude limit the sensitivity of the system when it is operated in a field applied by a handwound external solenoid rather than by the integrated field coils.

The gradiometric pickup loops and like-polarity field coils form the ends of a symmetric common axis, the susceptometer axis, which extends 1.2 mm in length [Fig. 2(a)]. The SQUID junctions and modulation coils are at the center of the susceptometer [Fig. 2(b)] placed symmetrically between the pickup loop/field coil pairs. The pickup loops are connected to the SQUID core by low-inductance planar coaxial lines that taper to a narrow point in the vicinity of the pickup loops [Fig. 2(c)]. The SQUID bias leads are also realized as a planar coaxial structure.

The flux coupling geometry at the center of the susceptometer has been designed to allow one to couple controlled flux from dedicated modulation coils to a SQUID that is primarily a self-shielded planar transmission line. Ketchen and Kirtley[14] have described the importance of shielding the sensor from parasitic coupling (through connecting leads and/or gaps between layers). We follow a similar design philosophy, but take advantage of improvements in lithography to reduce sharp corners by tapering the tip at a shallow angle (14° half-angle). The field coil leads are shielded by a floating superconducting strip of sufficient width (10 μm) to overlap both leads. The shielding of the pickup loop leads is more complicated due to the transition from a fully planar coaxial geometry to the bare pickup loop. One lead is the center conductor of the coaxial geometry and the other lead is the outer conductor. The leads are shielded by a single layer of superconducting film (above) tied to the coaxial shield for a distance of 12 μm, and by two layers of superconducting film (above and below) also tied to the coaxial shield for a distance of 35 μm. Of this "dual-shielded" segment, 15 μm of the length is additionally shielded by floating extensions of the coaxial shield in the same layer as the pickup loop leads. The combination of shielding features results in a reasonably symmetrical imaging kernel.

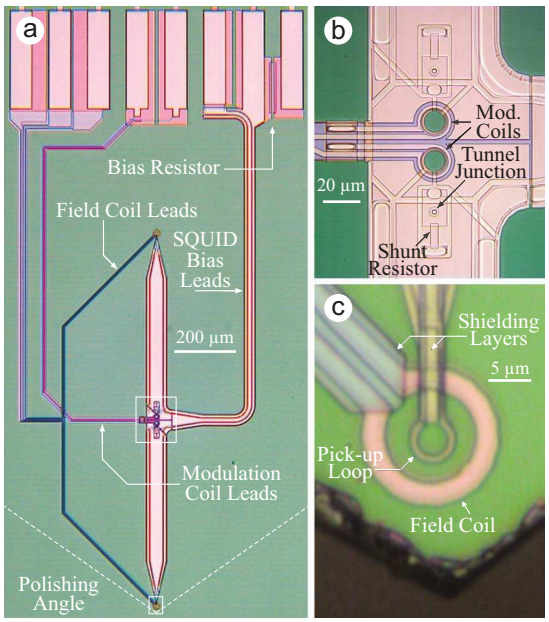

FIG. 2. (Color online) (a) Photomicrograph of the full device, prior to polishing the tip. Material below the white dashed line is removed during polishing. Pads for wirebonding are at the top. The distance between pickup loops is 1.2 mm. The area enclosed by the box near the center of the SQUID is enlarged in (b), and the area enclosed by the box near the tip is enlarged in (c). (b) Close-up view of the core area of the SQUID, including junctions, shunt resistors, and modulation coils. (c) Close-up view of the sensor area, after polishing. Note shielding layers above both the pickup loop leads and the field coil leads.

The SQUID fabrication uses a conventional $Nb/AlO_x/Nb$ trilayer Josephson junction technology, including PdAu shunt resistors, SiO_2 dielectric interlayers, and Nb wiring layers. The Nb and Al are deposited by dc sputtering in an Ar atmosphere, the PdAu resistors are deposited by electron-beam evaporation, and the SiO_2 interlayer is deposited by electron cyclotron resonance plasma enhanced chemical vapor deposition (ECR PECVD). A full description of this process is given elsewhere.[19] Device features were defined in an optical lithography process with approximately 0.8 μm minimum feature size and 1 μm minimum feature spacing.

III. EXPERIMENTAL SYSTEM

The field coil leads are oriented at a 45° angle to the axis of the SQUID, allowing the susceptometer chip to be polished to within approximately 15 μm of the field coil ($\approx$25 μm from the center of the pickup loop), placing the pickup loop near the edge of the substrate [Fig. 2(c)]. The device is then fastened to a cantilever and aligned at an angle of approximately 2° with respect to the sample plane. With this alignment, the pickup loop can be positioned in close proximity (25 μm $\times \sin 2° \approx 1$ μm) to the sample. The can-

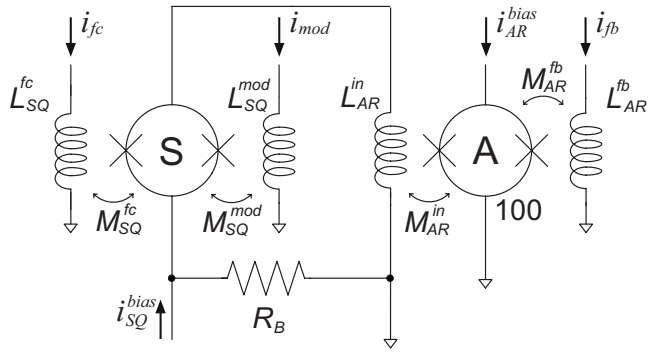

FIG. 3. Circuit diagram for the device operation. Local compensated field coils apply magnetic field to the two ends of the SQUID susceptometer (S) with coupling $M_{SQ}^{fc}=1.0\Phi_0/mA=2.1$ pH. Modulation coils with $M_{SQ}^{mod}=16\Phi_0/mA=33$ pH allow for additional feedback circuitry to keep the device at an optimal working flux bias, while linearizing the response to an applied field. The susceptometer is voltage biased through $R_B\approx 100$ mΩ and the SQUID current is coupled to a series array SQUID preamplifier (A) with input mutual inductance $M_{AR}^{in}=33\Phi_0/mA=68$ pH. The flux bias of S is set through an offset voltage in the feedback circuitry, and the flux bias of A is set through the mutual inductance $M_{AR}^{fb}=4.2\Phi_0/mA=8.7$ pH.

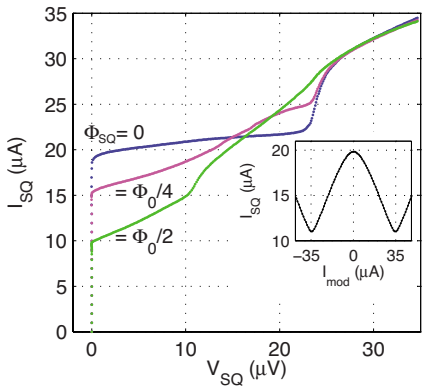

FIG. 4. (Color online) Operating characteristics of the SQUID susceptometer. Main graph: Current-voltage characteristics of the SQUID at various flux bias points Inset: SQUID current, I_{SQ}, as a function of the modulation coil current I_{mod} which couples flux through the modulation coils rather than the pickup loop. The voltage bias at this operating point is ~ 2 μV.

tilever movement is controlled by a large area scanning piezoelectric S-bender[20] with additional coarse motion control by slip-stick motion positioners.[21]

We voltage bias the SQUID and read out the current with a SQUID array preamplifier to improve performance (Fig. 3). The advantage to using a SQUID series array preamplifier is that its output impedance is designed to couple well to room-temperature electronics. Thus, there is no need for an impedance-matching transformer, and the feedback circuit can be directly coupled, without use of a modulation frequency. We use a $N=100$ SQUID series array[22] with an output impedance of ~ 300 Ω. When the array is operated in a magnetically shielded environment, a minimal amount of flux trapping occurs and the combined dc output from all of the SQUIDs is essentially N times the dc output from a single SQUID.

Since the SQUID array preamplifier is a low-input-impedance device, it is more natural to voltage bias the susceptometer and read out its current with the SQUID array. The input current sensitivity of the SQUID series array is approximately 2.5 pA/$\sqrt{\text{Hz}}$ with a $1/f$ knee at ~ 50 Hz. This measured noise is less than the fundamental noise of the susceptometer and ensures that we realize the full intrinsic sensitivity of the susceptometer.

Moreover, the intrinsic bandwidth of the SQUID series array with an open-circuit on the input coil is greater than 100 MHz.[22] The bandwidth of our room temperature electronics is approximately 5 MHz. In principle, the frequency response of the susceptometer with preamplifier is limited by the L_{AR}^{in}/R_{dyn} time constant of the SQUID array input inductance L_{AR}^{in} and susceptometer dynamic resistance R_{dyn}. The measured bandwidth of the present arrangement (1 MHz) is consistent with measured values of L_{AR}^{in} and R_{dyn}.

IV. NOISE DESIGN AND PERFORMANCE

In order to minimize the SQUID flux noise, we followed a design prescription[23] which sets the Josephson junction critical current I_c based on the SQUID self-inductance L_{SQ} through the relation $I_c=\Phi_0/2L_{SQ}$. Numeric modeling[18] was used to estimate the inductance of individual SQUID components yielding: modulation core region, 55 pH; strip line, 9 pH/mm; taper region, 4 pH; and pickup loop, 13 pH. The combined inductance $L_{SQ}\approx 100$ pH agrees to within experimental uncertainty with the actual inductance, as extrapolated[24] from the critical currents at applied flux values of $\Phi_{SQ}=0$ and $\Phi_0/2$. The designed single-junction value $I_c\approx 10$ μA agrees well with the measured maximum SQUID critical current $I_{c,SQ}^{max}/2$, as shown in Fig. 4. Using the same design prescription, shunted dc SQUIDs are nonhysteretic when the parameter $\beta_C=2\pi I_c R_{shunt}^2 C_J/\Phi_0\leqslant 1$, where R_{shunt} is the junction shunt resistance and C_J is the capacitance of each junction. We report on our highest resistance ($R_{shunt}=2.4$ Ω) devices that have a nonhysteretic response. The nominal design values are $\beta_L=2I_cL_{SQ}/\Phi_0=1$ and $\beta_C=0.2$. The dynamic resistance under a typical operating bias is approximately 3.5 Ω.

A bias resistor of approximately 100 mΩ is fabricated on the same substrate as the susceptometer. This resistor need not be used if local heating is a concern or if simpler wiring is preferred. For example, we use a discrete resistor heat sunk to the 1 K pot for dilution refrigerator operation.

The frequency-independent (white) flux sensitivity of dc SQUIDs has been thoroughly analyzed with respect to design parameters.[23] Figure 5(b) shows this flux noise (as measured between 20 and 30 kHz) as a function of temperature for one of our typical devices. One contribution to this noise is Johnson noise in the shunt resistors. This noise is minimized when $\beta_L\sim 1$ and $\beta_c=1$, giving a theoretical limit[25] of $\Phi_n=\sqrt{S_\Phi}=(16k_BTL_{SQ}\sqrt{L_{SQ}C_J})^{1/2}$. Above 0.5 K, the device noise has the same functional dependence on the temperature and is only slightly larger in magnitude than this limit, in accordance with the reduced β_c parameter. When the temperature is reduced below 0.5 K, the flux noise plateaus at a value (0.25 $\mu\Phi_0/\sqrt{\text{Hz}}$) higher than the quantum limit.[26] This behavior is consistent with an electron temperature saturation caused by weak electron-phonon coupling at low temperatures as described by Wellstood.[27] This white-noise flux sensitivity corresponds to an equivalent spin sensitivity for samples located in the plane of, and at the center of, the

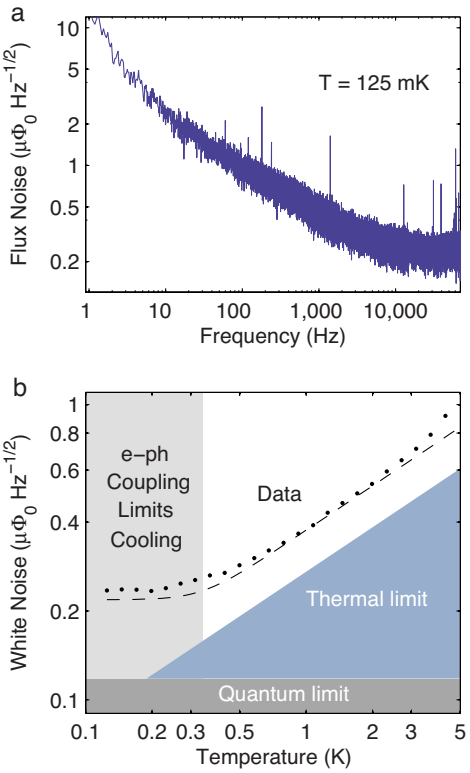

FIG. 5. (Color online) (a) Noise spectrum observed in a functional scanning setup at 125 mK. The low frequency ($1/f$-like) noise is believed to be associated with the magnetic field of spins, as discussed in the text. The rms white noise floor is approximately $0.25\mu\Phi_0/\sqrt{\text{Hz}}$. (b) White noise floor (points) as a function of temperature. The shaded areas represent the quantum and thermal noise limits for the optimal performance of a resistively shunted device with an inductance of 100 pH. The dashed line represents a fit to the Johnson noise temperature dependence that includes the effect of weak electron-phonon interactions limiting the minimum electron temperature to ~400 mK.

pickup loop of 200 $\mu_B/\sqrt{\text{Hz}}$. The actual spin sensitivity will vary depending on the position of the sample relative to this reference point,[14] and the given value is presented as a figure of merit only.[17]

The $1/f$-like low frequency noise [Fig. 5(a)] is typically about $2.5\mu\Phi_0/\sqrt{\text{Hz}}$ at 10 Hz, and depends on frequency approximately as $\Phi_n=\sqrt{S_\Phi}\propto f^{-0.35}$ rather than $\sqrt{S_\Phi}\propto f^{-0.5}$. We have verified that it does not come from the SQUID series array or room temperature amplifier stages. There is only very weak temperature dependence. Tests using a bias reversal scheme[5] indicate that this low frequency noise is true flux noise, rather than due to critical current fluctuations. Similar $1/f$ flux noise levels have been reported for other devices.[28]

V. COUPLING TO MESOSCOPIC SAMPLES

Our sensor is designed to measure weak magnetic signals from mesoscopic objects (Fig. 6). To locate these small objects, large magnetic features must be included in the lithography. The sample in Fig. 6(a) includes aluminum rings and a gold meander wire to indicate each ring's position. Current through the grid of meander wires generates magnetic field that can be imaged with the susceptometer's pickup coil [Fig. 6(b)]. Notches in the grid represent binary bits that differentiate one grid section from the next. Below

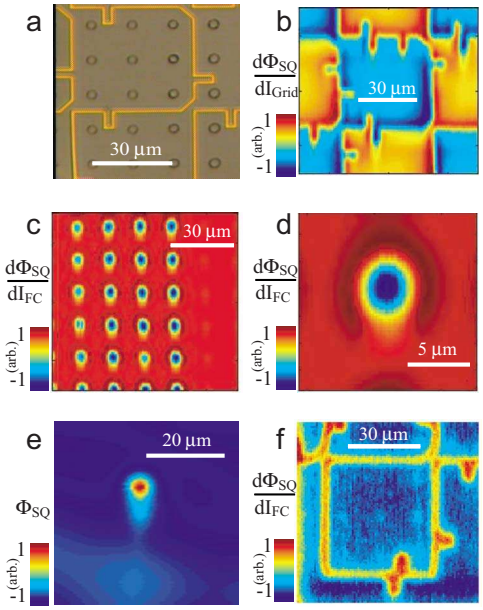

FIG. 6. (Color online) (a) Optical micrograph of a sample with aluminum rings and a gold meander wire. (b) Lock-in measurement of flux resulting from a current carried through the meander wire. This is a different grid section than in (a). (c) Response of several superconducting rings to magnetic field applied by the field coils (susceptibility scan). (d) Higher resolution image of a single ring showing the sensor's imaging kernel in susceptibility mode. (e) Image of a single superconducting vortex in niobium, demonstrating the magnetometry imaging kernel. (f) Susceptibility scan of the grid lines (with zero grid current) at 32 mK. The response is consistent with a 50 ppm concentration of $s=1/2$ spins.

the superconducting transition temperature for aluminum, the rings have a strong diamagnetic response to an applied field generated by the field coil [Fig. 6(c)]. A higher resolution scan of a single ring [Fig. 6(d)] shows the imaging kernel of the sensor in susceptibility mode. The dark area around the ring represents a weak negative coupling when the ring is directly next to the pickup loop and the returning field lines thread the sensor area. The magnetometry response to an isolated vortex pinned in a niobium thin film sample [Fig. 6(e), near zero applied field] represents the typical response to a sharp feature with its own intrinsic monopolelike magnetic field. Figure 6(f) shows the response from a sample like the one shown in Fig. 6(a) but composed of normal metal Au rings instead of the superconducting Al, and where an AlO_x insulator exists above the grid lines and below the rings. At the lowest temperatures (~30 mK) a paramagnetic susceptibility associated with spins in the metal and/or this insulating layer[29] is visible after averaging times of a few to several tens of minutes.

Once scanning has been used to identify a specific sample on a multi-sample substrate [Fig. 7(a)], the sensor can be used to make *in situ* background measurements, allowing for the acquisition of a full I-Φ curve. This procedure involves measuring the nonlinear SQUID response as a function of the applied field [Fig. 7(b)] at various distances from the sample in question. We usually apply a sinusoidal current to the field coils to avoid high frequency components, which would be more affected by the finite measurement bandwidth. The counterwound design leads to the initial two orders of magnitude of cancellation of the applied flux, as de-

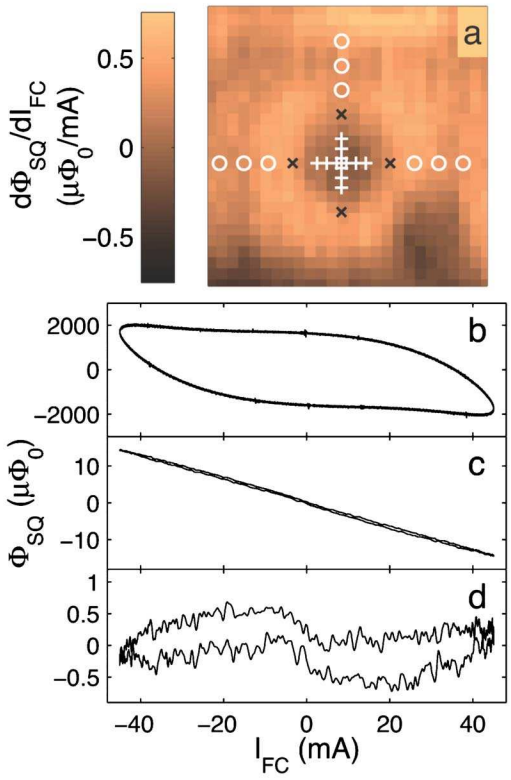

FIG. 7. (Color online) (a) Lock-in measurement of the SQUID response to current applied by the field coil. The cross marks are centered on the susceptibility response of a gold ring with a sample structured similar to Figs. 6(a) and 6(f). The white circles and plus marks indicate positions sampled for weighted background subtraction. (b) Set of Φ_{SQ}-I_{FC} curves taken at all the points indicated in (a). The data are indistinguishable at this scale. (c) SQUID response after the points off of the ring (white circles) are subtracted from the points centered over the ring (white plus marks), weighted by the SQUID's response kernel. (d) Subtracting a fitted linear response, presumably from spins in the ring, leaves a nonlinear response which we attribute to nonequilibrium effects in the metal.

scribed above. After nulling the linear in-phase component of this response by feeding an adjustable current into the center tap, we typically find a residual signal on the order of 10^{-4} times the bare applied flux. This residual signal [Fig. 7(b)] consists mostly of an out-of-phase component, which arises as the difference of two large signals of equal amplitude with a very slight phase shift. Particularly at a large applied field, a nonlinear component that we attribute to current induced pair breaking in or near the field coils becomes visible. To distinguish this sensor background from the much smaller sample signal, we measure it *in situ* by moving the pickup loop away from the sample and subtracting the result from that obtained when coupled to the sample [Fig. 7(c)]. Our best results were obtained when moving the scanner on and off the sample parallel to the substrate, and measuring about 1 s at each position, so that the background susceptibility from the substrate is also eliminated, and slow variations in the sensor background are averaged out. With this procedure, we were able to obtain a nonlinear response of less than $0.1\mu\Phi_0$ at a field coil current of 45 mA (corresponding to about $45\Phi_0$ or 45 G) after averaging for 38 h above a region of bare silicon substrate and subtracting the linear component [Fig. 7(d)].[29] The latter was at least partly due to the susceptibility of nearby metal patterned on the substrate. Thus, we have achieved a cumulative background rejection of better than 8.5 orders of magnitude. Moreover, this sensitivity after averaging is consistent with the previously measured noise level (Fig. 5), demonstrating that these measurements can be made at the full sensitivity of the sensor.

VI. CONCLUSION

We have characterized a Nb high-symmetry scanning SQUID susceptometer between 0.025 and 6 K. The spectral density of the flux noise in the frequency-independent region is $0.25\mu\Phi_0/\sqrt{\text{Hz}}$ below ~200 mK, equivalent to a spin sensitivity of approximately $200\mu_B/\sqrt{\text{Hz}}$ for samples at the center of, and in the plane of, the pickup loop. This device has better than 100 times greater spin sensitivity than our previous device.[15] The improved performance is due to the reduced pickup loop dimensions, improved shielding, and improved symmetry with regard to the SQUID and field coil placement, and voltage biasing techniques on the readout stage. As expected, the limiting factor in bandwidth is set by the array input loop and the dynamic resistance of the SQUID susceptometer. The ability to position the sensor over multiple samples in a given cryogenic run and the ability to isolate the sensor from the samples for background subtraction combine to maximize the device utility and sensitivity.

ACKNOWLEDGMENTS

This work was supported by the Stanford-IBM Center for Probing the Nanoscale (CPN), an NSF NSEC, Grant No. PHY-0425897; by the Packard Foundation; and by NSF Grant Nos. DMR-0507931, DMR-0216470, and ECS-0210877. We thank J. R. Kirtley and K. D. Irwin for useful discussions. We thank J. A. Bert for useful discussions and comments on drafts of this paper. We also acknowledge the use of the microfabrication facilities of the National Institute of Standards and Technology in Boulder, CO.

[1] N. C. Koshnick, H. Bluhm, M. E. Huber, and K. A. Moler, Science **318**, 1440 (2007).
[2] W. A. Little and R. D. Parks, Phys. Rev. Lett. **9**, 9 (1962).
[3] H. Bluhm, N. C. Koshnick, M. E. Huber, and K. A. Moler, arXiv:cond-mat/0709.1175.
[4] H. Bluhm, N. C. Koshnick, M. E. Huber, and K. A. Moler, Phys. Rev. Lett. **97**, 237002 (2006).
[5] *The SQUID Handbook*, edited by J. Clarke and A. I. Braginski (Wiley-VCH, Weinheim, 2003).
[6] D. Mailly, C. Chapelier, and A. Benoit, Phys. Rev. Lett. **70**, 2020 (1993).
[7] M. B. Ketchen, T. Kopley, and H. Ling, Appl. Phys. Lett. **44**, 1008 (1984).
[8] X. Zhang and J. C. Price, Phys. Rev. B **55**, 3128 (1997).
[9] W. Wernsdorfer, K. Hasselbach, D. Mailly, B. Barbara, A. Benoit, L. Thomas, and G. Suran, J. Magn. Magn. Mater. **145**, 33 (1995).
[10] S. K. H. Lam and D. L. Tilbrook, Appl. Phys. Lett. **82**, 1078 (2003).
[11] A. G. P. Troeman, H. Derking, B. Borger, J. Pleikies, D. Veldhuis, and H. Hilgenkamp, Nano Lett. **7**, 2152 (2007).
[12] J.-P. Cleuziou, W. Wernsdorfer, V. Bouchiat, T. Ondarcuhu, and M. Monthioux, Nat. Nanotechnol. **1**, 53 (2006).
[13] J. R. Kirtley, M. B. Ketchen, K. G. Stawiasz, J. Z. Sun, W. J. Gallagher, S. H. Blanton, and S. J. Wind, Appl. Phys. Lett. **66**, 1138 (1995).
[14] M. B. Ketchen and J. R. Kirtley, IEEE Trans. Appl. Supercond. **5**, 2133 (1995).
[15] B. W. Gardner, J. C. Wynn, P. G. Bjornsson, E. W. J. Straver, K. A. Moler, J. R. Kirtley, and M. B. Ketchen, Rev. Sci. Instrum. **72**, 2361 (2001).

[16] M. B. Ketchen, W. J. Gallagher, A. W. Kleinsasser, S. Murphy, J. R. Clem, in *SQUID '85: Superconducting Quantum Interference Devices and their Applications*, edited by H. D. Hahlbohm and H. Lübbig (Walter de Gruyter & Co., Berlin, 1985), pp. 865–871.
[17] M. B. Ketchen, D. D. Awschalom, W. J. Gallagher, A. W. Kleinsasser, R. L. Sandstrom, J. R. Rozen, and B. Bumble, IEEE Trans. Magn. **25**, 1212 (1989).
[18] M. Kamon, M. J. Tsuk, and J. K. White, IEEE Trans. Microwave Theory Tech. **42**, 1750 (1994).
[19] J. E. Sauvageau, C. J. Burroughs, P. A. A. Booi, M. W. Cromar, S. P. Benz, and J. A. Koch, IEEE Trans. Appl. Supercond. **5**, 2303 (1995).
[20] J. Siegel, J. Witt, N. Venturi, and S. Field, Rev. Sci. Instrum. **66**, 2520 (1995).
[21] attocube systems AG, URL www.attocube.com
[22] M. E. Huber, P. A. Neil, R. G. Benson, D. A. Burns, A. F. Corey, C. S. Flynn, Y. Kitaygorodskaya, O. Massihzadeh, J. M. Martinis, and G. C. Hilton, IEEE Trans. Appl. Supercond. **11**, 4048 (2001).
[23] C. D. Tesche and J. Clarke, J. Low Temp. Phys. **29**, 301 (1977).
[24] R. L. Peterson and C. A. Hamilton, J. Appl. Phys. **50**, 8135 (1979).
[25] C. D. Tesche and J. Clarke, J. Low Temp. Phys. **37**, 397 (1979).
[26] R. H. Koch, D. J. V. Harlingen, and J. Clarke, Appl. Phys. Lett. **38**, 380 (1981).
[27] F. C. Wellstood, C. Urbina, and J. Clarke, Phys. Rev. B **49**, 5942 (1994).
[28] F. C. Wellstood, C. Urbina, and J. Clarke, Appl. Phys. Lett. **50**, 772 (1987).
[29] H. Bluhm, N. C. Koshnick, J. Bert, M. E. Huber, and K. A. Moler (unpublished).